Highly porous seeding-free boron-doped ultrananocrystalline diamond used as high-performance anode for electrochemical removal of carbaryl from water

Laís G Vernasqui, Alexsandro J dos Santos, Guilherme V Fortunato, Matheus S Kronka, Haruna L Barazorda-Ccahuana, Ana S Fajardo, Neidenêi G Ferreira, Marcos R.V. Lanza

Highly porous seeding-free boron-doped ultrananocrystalline diamond used as high-performance anode for electrochemical removal of carbaryl from water

Laís G. Vernasqui[a], Alexsandro J. dos Santos[b*], Guilherme V. Fortunato[b], Matheus S. Kronka[b], Haruna L. Barazorda-Ccahuana[c], Ana S. Fajardo[d,e], Neidenêi G. Ferreira[a], Marcos R. V. Lanza[b*]

[a]*National Institute for Space Research – INPE, Av. dos Astronautas, 1758, Jd. Granja, São José dos Campos, SP, 12227-010, Brazil*

[b]*São Carlos Institute of Chemistry, University of São Paulo, Avenida Trabalhador San-Carlense 400, São Carlos, SP 13566-590, Brazil*

[c]*Vicerrectorado de Investigación, Universidad Católica de Santa María, Urb. San José s/n - Umacollo, Arequipa, 04000, Perú*

[d]*Nanosystems Engineering Research Center for Nanotechnology-Enabled Water Treatment, School of Sustainable Engineering and the Built Environment, Arizona State University, Tempe, AZ 85287-3005, USA*

[e]*Sorbonne Université, CNRS, Laboratoire Interfaces et Systèmes Electrochimiques (LISE), 4 place Jussieu, F-75005, Paris, France*

Corresponding authors:

alexsandrojhones@usp.br (A. J. dos Santos)

marcoslanza@usp.br (M.R.V. Lanza)

Abstract

Boron-doped diamond (BDD) electrodes are regarded as the most promising catalytic materials that are highly efficient and suitable for application in advanced electrochemical oxidation processes targeted at the removal of recalcitrant contaminants in different water matrices. Improving the synthesis of these electrodes through the enhancement of their morphology, structure and stability has become the goal of the material scientists. The present work reports the use of an ultranano-diamond electrode with a highly porous structure (B-UNCD$_{WS}$/TDNT/Ti) for the treatment of water containing carbaryl. The application of the proposed electrode at current density of 75 mA cm^{-2} led to the complete removal of the pollutant (carbaryl) from the synthetic medium in 30 min of electrolysis with an electric energy per order of 4.01 kWh m^{-3} order^{-1}. The results obtained from the time-course analysis of the carboxylic acids and nitrogen-based ions present in the solution showed that the concentrations of nitrogen-based ions were within the established maximum levels for human consumption. Under optimal operating conditions, the proposed electrode was successfully employed for the complete removal of carbaryl in real water. Thus, the findings of this study show that the unique, easy-to-prepare BDD-based electrode proposed in this study is a highly efficient tool which has excellent application potential for the removal of recalcitrant pollutants in water.

Keywords: Recalcitrant pollutants; Water treatment; Advanced oxidation processes; Electrochemical technologies; Boron-doped diamond synthesis.

1. Introduction

Anodic oxidation (AO) is one of the major electrochemically-driven technologies which have been widely applied for the remediation of recalcitrant organic substances - including dyes, personal care and pharmaceutical products, and pesticides, usually present in water bodies (Sirés and Brillas, 2012; Sirés et al., 2014; Baddouh et al., 2018; Garcia-Segura et al., 2018b; Martínez-Huitle and Panizza, 2018; dos Santos et al., 2021b;). AO is considered an environmentally friendly technique as the process does not require the use of chemicals and oxidants are electrogenerated *in situ*. Several studies have shown that the electrocatalytic properties of the anode material are among the main factors that determine the efficiency of the AO process (Panizza and Cerisola, 2009; Sirés et al., 2014; Moreira et al., 2017; dos Santos et al., 2019, 2021a). In this context, boron-doped diamond (BDD) anode is regarded as the best material for application in AO due to its excellent properties including high stability, inert surface, and large O_2 overpotential window (Kapałka et al., 2009). The large O_2 overpotential window of BDD anode helps generate a huge amount of oxidant species such as physiosorbed hydroxyl radicals (M($^{\bullet}$OH), Eq. (1) which can attack organic pollutants (R) non-selectively, turning them into non-hazardous products or even leading them to complete combustion, as shown in Eq. (2) below (do Vale Júnior et al., 2019; Brillas, 2021; Karim et al., 2021; Mostafa et al., 2021).

$$M + H_2O \rightarrow M(^{\bullet}OH) + H^+ + e^- \quad (1)$$

$$aM(^{\bullet}OH) + R \rightarrow mCO_2 + nH_2O + xH^+ + ye^- \quad (2)$$

The properties of BDD can be enhanced considerably by varying the concentration of boron, film thickness, and sp^2/sp^3 ratio, as well as the electrode morphology and porosity (Baluchová et al., 2019; Mei et al., 2019). As pointed out in the literature, one can promote the contact between the electrolyte and the electrode by increasing the electrochemical surface area through the adjustment of the film porosity from macro to nano-porous depending on both the porosity of the substrate and specific post-growth treatment on the diamond surface. So far, a number of studies reported in the literature have employed the seeding substrate pre-treatment mechanism to boost the diamond growth through the application of the chemical vapor deposition technique (Wei et al., 2009; Szunerits et al., 2015; Yang et al., 2016). This pre-treatment mechanism involves the use of diamond powder to improve diamond growth since diamond is unable to grow naturally on non-diamond substrates. Due to the fast deposition kinetics, this seeding substrate pre-treatment procedure, which boosts the diamond growth, favors the formation of agglomerated structures; on the other hand, the fast deposition

kinetics makes it harder to obtain structures with nano or ultranano-porosity which are more suitable and efficient for improving the efficiency of the AO process (May and Mankelevich, 2008; Luong et al., 2009; Macpherson, 2015).

As an alternative to the typical BDD synthesis method, in a previous study (Vernasqui et al., 2022), our research group proposed the use of an innovative boron-doped ultrananocrystalline diamond grown on titanium dioxide nanotube without the seeding substrate pre-treatment procedure (B-UNCD$_{ws}$/TDNT/Ti). The use of titanium dioxide nanotubes (TDNT) allows spontaneous diamond growth under slower deposition kinetics compared to the seeding process, and this enables one to have higher control of deposition and the ability to produce extremely thin films, in addition to maintaining the porosity of the substrate material. This approach represents a major step forward in the synthesis of BDD and helps explore the unique properties of BDD when it comes to the treatment of recalcitrant pollutants. Thus, this study evaluates the efficiency of the innovative B-UNCD$_{ws}$/TDNT/Ti electrode when applied for the removal of carbaryl (CBR) pesticide in both synthetic and real media under the AO process. Carbaryl is a broad-spectrum N-methyl carbamate insecticide applied worldwide for the control of pests during the production of crops (cotton, corn, soybean, nut, fruits, and vegetables) and for the protection of lawns, home gardens and other ornamental plants (Koshlukova and Reed, 2014).

CBR ranks second among the insecticides that are commonly detected in surface water (Nair et al., 2022). CBR can dissolve in water, migrate through soil, and find its way into groundwater, contaminating it (Wu et al., 2019). People are mostly exposed to CBR through the intake of food and water or other liquids. Depending on the individual and the dose of CBR ingested into the body, the person may experience a variety of symptoms which range from weakness to reduced heart and lung function. In view of that, it is essentially important to develop techniques that are capable of removing this type of contaminant from food and water so as to prevent excessive human exposure to this pollutant and the occurrence of severe health problems in humans. To analyze the efficiency and viability of the proposed anode in terms of CBR degradation, different current densities were tested, and the best operating conditions were applied for the analysis of real drinking water with a view to evaluating the potential of the technique in real applications. The presence of different oxidants in the system was evaluated using scavenger compounds. Energetic figures of merit were calculated, and the evolution of intermediates produced during the treatment process was also thoroughly monitored. For

comparison purposes, the study also provides comprehensive data related to the physical and electroanalytical characterization of the proposed B-UNCD$_{WS}$/TDNT/Ti anode.

2. Materials and methods

2.1 Chemical reagents

Carbaryl (CBR) pesticide (99 % purity, Sigma-Aldrich) was used as a model pollutant. Analytical grade potassium sulfate – acquired from Neon, was used as supporting electrolyte; methanol (MeOH) and *tert*-butanol (TBH), both acquired from Sigma Aldrich, were used as scavengers; and acetonitrile – obtained from Merck, was used as mobile phase for the conduct of high-performance liquid chromatography (HPLC) analysis. All reagents were used directly without extra purification. Ultrapure water from a Millipore Milli-Q system (electric resistivity >18 MΩ cm at 25 °C) was used to prepare the aqueous solutions.

2.2 B-UNCD$_{WS}$/TDNT/Ti synthesis and characterization

The synthesis of the B-UNCD$_{WS}$/TDNT/Ti electrode was performed under a two-step approach. The first step involved obtaining anodized TDNTs and the second step involved the deposition of diamond through the application of the hot filament chemical vapor deposition (HFCVD) technique as described by (Vernasqui et al., 2022). A commercial microcrystalline BDD thin film doped on a silicon substrate (acquired from NeoCoat) were employed for comparison purposes. The synthesized anode material (B-UNCD$_{WS}$/TDNT/Ti) was analyzed by field emission gun scanning electron microscopy (FEG-SEM, TESCAN Mira 3), Raman scattering spectroscopy - using 514.5 nm line of argon ion-laser (Lab- RAMHR evolution from Horiba Scientific), and X-ray diffraction (XDR – PANanalytical model X'Pert Pro MPD diffractometer with CuK_α radiation). Cyclic voltammetry (CV), linear scan voltammetry (LSV), and electrochemical impedance spectroscopy (EIS) measurements were performed using N_2-satured H_2SO_4 or K_2SO_4 solutions with the aid of an Autolab PGSTAT128N potentiostat/galvanostat equipped with FRA2.X module. The electrochemical assays were carried out in a three-electrode electrochemical cell which consisted of the following: B-UNCD$_{WS}$/TDNT/Ti, Pt plate (Degussa) and Ag/AgCl (~3.0 M *KCl*, Analyser Co.) used as working, counter, and reference electrodes, respectively. The specific capacitance values were determined by the double-layer capacitance (C_{dl}) method as described in (McCrory et al., 2013). The LSV analyses were performed in a potential window ranging from 0 to 3.0 V *vs.* Ag/AgCl at scan rate of 20 mV s^{-1}. The impedance analyses were conducted at 2.3 V *vs.* Ag/AgCl, with potential perturbation of 25 mV (rms) and frequency range of 10 mHz to 100 kHz. The EIS data were analyzed using an electric equivalent circuit (EEQC) with the aid of the Nova®

2.1.4 software. Water contact angle measurements were performed using Attension Theta Flex tensiometer by pouring water droplets (of 5 µL) on the B-UNCD$_{WS}$/TDNT/Ti electrode.

2.3 Anodic oxidation experimental setup and analytical techniques

The electrochemical treatment of CBR in 50 mM K_2SO_4, at pH = 7.0, was carried out in a 250 mL lab-scale glass reactor operated at 400 rpm magnetic stirring rate, at 25 ˚C. The anode/cathode pair employed for the conduct of the experiments was as follows: B-UNCD$_{WS}$/TDNT/Ti (geometric area of 2.0 cm^2) – as anode, and a platinum wire – as cathode. The electrodes were positioned vertically with 1.0 cm distance between them. All experiments were performed at constant current density (*j*) using a power supply from MINIPA (MPL-3305). Prior to the conduct of each experiment, the electrodes were cleaned using a 50 mM K_2SO_4 solution at *j*=100 mA cm^{-2} for 20 min. The drinking water used in the experiments was obtained from the water treatment plant in the city of Bariri, São Paulo State, Brazil – the effluent was stored at 4 °C. Table 1 shows the physical chemical characterization of the real effluent. At predetermined periods of time (0, 5, 10, 15, 20, 30, 40, 50 and 60 min), the samples were collected, filtered, and injected into the Shimadzu High-Performance Liquid Chromatograph (HPLC) for the analysis of the rate/degree of carbaryl removal. A C18 column (250×4.6, 5 µm) was used for the HPLC analysis, and the mobile phase employed consisted of a mixture of water/acetonitrile (ratio 60:40) applied at a flow rate of 1.0 mL min^{-1}.The electric energy per order (EE/O), a figure of merit established by the IUPAC (Lanzarini-Lopes et al., 2017), was estimated based on Eq. (3) in order to determine the economic viability of the AO process.

$$EE/O = (kWh\, m^{-3} order^{-1}) = \frac{E_{cell} I t}{V_s log(c_0/c_f)} \quad (3)$$

where E_{cell} is the cell potential (V), I is the current intensity (A), t is the experiment time (s), Vs is the solution volume (L), and c_0 and c_f correspond to the initial and final concentrations of CBR (Garcia-Segura et al., 2018). The mineralization of the pollutant was evaluated by the Total Organic Carbon (TOC) technique using the Shimadzu VCPN TOC equipment. Carboxylic acids and nitrogenous species were detected using the Metrohm Ion Chromatography system, as described by (dos Santos et al., 2021a).

Table 1. Physical-chemical characterization of the drinking water employed in the experiments.

Physical Characteristics	**Values**
pH	7.50
Conductivity (uS cm^{-1})	129.7
Total organic carbon (mg C L^{-1})	0.45
Chemical Characteristics	**Values (**mg L^{-1})
Ammonia (NH_4^+)	0.134
Calcium (Ca^{2+})	12.79
Magnesium (Mg^{2+})	2.94
Potassium (K^+)	1.23
Sodium (Na^+)	4.47
Chloride (Cl^-)	3.31
Nitrate (NO_3^-)	0.72
Sulfate (SO_4^{2-})	1.55

3. Results and discussion

3.1. Morphological, physical, and electrochemical characterizations of the B-UNCD$_{WS}$/TDNT/Ti

Figure 1(a-d) shows the remarkable homogeneous morphology of the UNCD$_{WS}$/TDNT/Ti with different growth planes obtained after chemical vapor deposition on TDNT in different magnifications. As can be observed, the entire surface of the electrode is covered by a thin layer, and one will notice the presence of a diamond film in the pore walls which helps maintain the porosity of the electrode surface. Furthermore, one can see clusters of ballas diamond which are distributed on the sample surface. In the XRD analysis (Fig. 1e), the crystalline peaks observed were identified as TiO_2, TiC, TiH, and Ti –based on the Inorganic Crystal Structure Database (ICSD: 9658, 044494, 044747, and 076144, respectively). The diamond peaks (111), (220), and (311) present in 2θ = 44.1º, 76.3º, and 91.9º can be found convoluted with other peaks (Ownby et al., 1992). The (220) preferential orientation in the diffractogram is related to the high nucleation process which is enhanced by the TiC – derived from the formation of TiO_2 on the TDNT substrate, present on the electrode surface (Vernasqui et al., 2022). Fig. 1f shows the Raman spectra obtained at the standard 514 nm wavelength. As expected, the sample exhibited a typical ultrananо-diamond behavior, with signal bands attributed to the formation of trans-poly-acetylene at around 1,150 and 1,490 cm^{-1} and a band at around 1,220 cm^{-1} which is attributed to the inclusion of boron in the diamond lattice, in addition to the usual G band (1,560 cm^{-1}, attributed to E_{2g} vibration). The diamond peak typically located at 1,332 cm^{-2} for microcrystalline films is completely hidden in the sample by the D band attributed to amorphous sp^2 bonds, which is usually expected for these

films. In addition, one will observe the presence of three other peaks at around 500, 650, and 880 cm^{-1} linked to B dimers vibrations (Mermoux et al., 2002; Crisci et al., 2008; dos Santos et al., 2022).

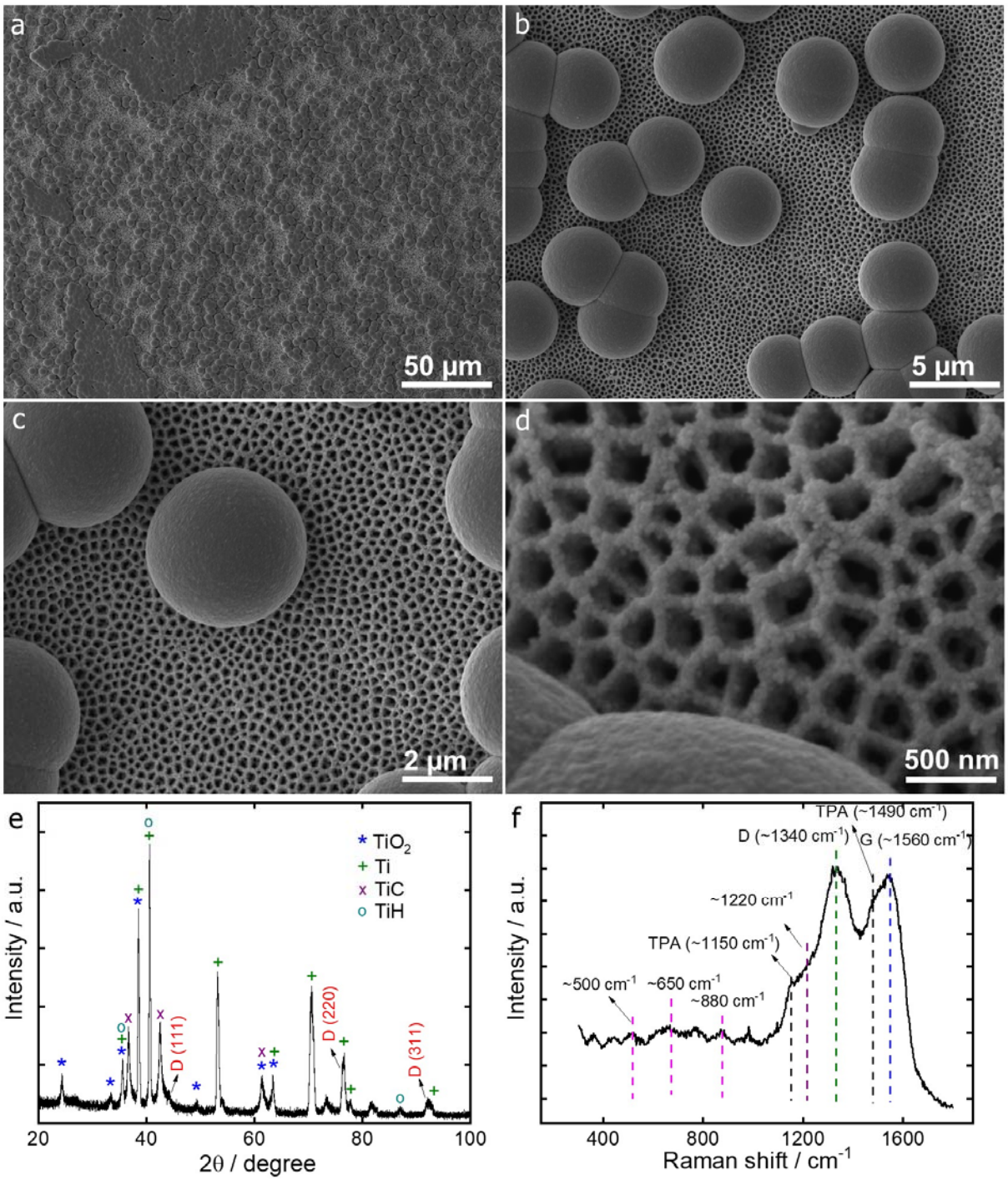

Fig 1. Physical characterization of the B-UNCD$_{WS}$/TDNT/Ti electrode. (a-d) Representative FEG-SEM images, (e) XRD pattern, and (f) Raman spectra.

Fig. 2a shows the capacitive features of the surface of the B-UNCD$_{WS}$/TDNT/Ti electrode which was evaluated in N_2–saturated 50mM H_2SO_4 solution. The CVs recorded at different scan rates in the double layer region (centered at the open circuit potential) point to the capacitive effect of the electrode. Based on the plot of average peak current *versus* scan rate in Fig. 2b, the B-UNCD$_{WS}$/TDNT/Ti electrode recorded specific capacitance of ca. 274 μF cm^{-2}; this value is higher than the specific capacitance value obtained for micro and nanocrystalline diamond films (115 μF cm^{-2}, on average) previously reported in the literature (dos Santos et al., 2022). The high specific capacitance values obtained for the electrode reflect the existence of high surface roughness and high active surface area, which provides the electrolyte solution access to the electrode surface (Frackowiak and Béguin, 2001; Siuzdak et al., 2015). The inset of Fig. 2b shows the hydrophobicity/wettability of the surface of the B-UNCD$_{WS}$/TDNT/Ti electrode; this was evaluated using the water contact angle measurement procedure. A water contact angle of ca. 87° shows that the B-UNCD$_{WS}$/TDNT/Ti material is a reasonably wettable substrate. A surface with intermediate wettability can provide the electrolyte solution easy access to the electrode surface and facilitated mass transport of gaseous species formed on the electrode surface which, when combined together, lead to the improvement of the electrolysis efficiency efficiency (Almeida et al., 2008; Watanabe et al., 2010). Linear scan voltammetry (LSV) measurements were recorded in N_2–saturated 50 mM K_2SO_4 solution, as shown in Fig. 2c. As can be observed, the B-UNCD$_{WS}$/TDNT/Ti electrode exhibited an onset potential for water discharge at 2.45 V *vs.* Ag/AgCl; this value is slightly higher than the values previously reported for diamond films with different morphologies (dos Santos et al., 2022) and for commercial microcrystalline BDD thin film - which exhibited an onset potential of 2.35 V *vs.* Ag/AgCl. Onset potential values for water discharge greater than 1.23 V *vs.* SHE (ca. 1.03 V *vs.* Ag/AgCl) are expected to favor the generation of reactive oxygen species (i.e $^{\bullet}OH$) rather than oxygen evolution during the electrolysis process (Kapałka et al., 2007). The seeding-free production of diamond allows the formation of highly porous ultranano-structures - which are in line with the surface characteristics of the substrate used, favoring the formation of extremely thin diamond films. In fact, this behavior is observed in the B-UNCD$_{WS}$/TDNT/Ti electrode, since an extremely thin-porous diamond film covering the TDNT gives rise to relatively lower current densities for water discharge compared to the current densities typically presented by micro- and nano-diamonds (dos Santos et al., 2022) .

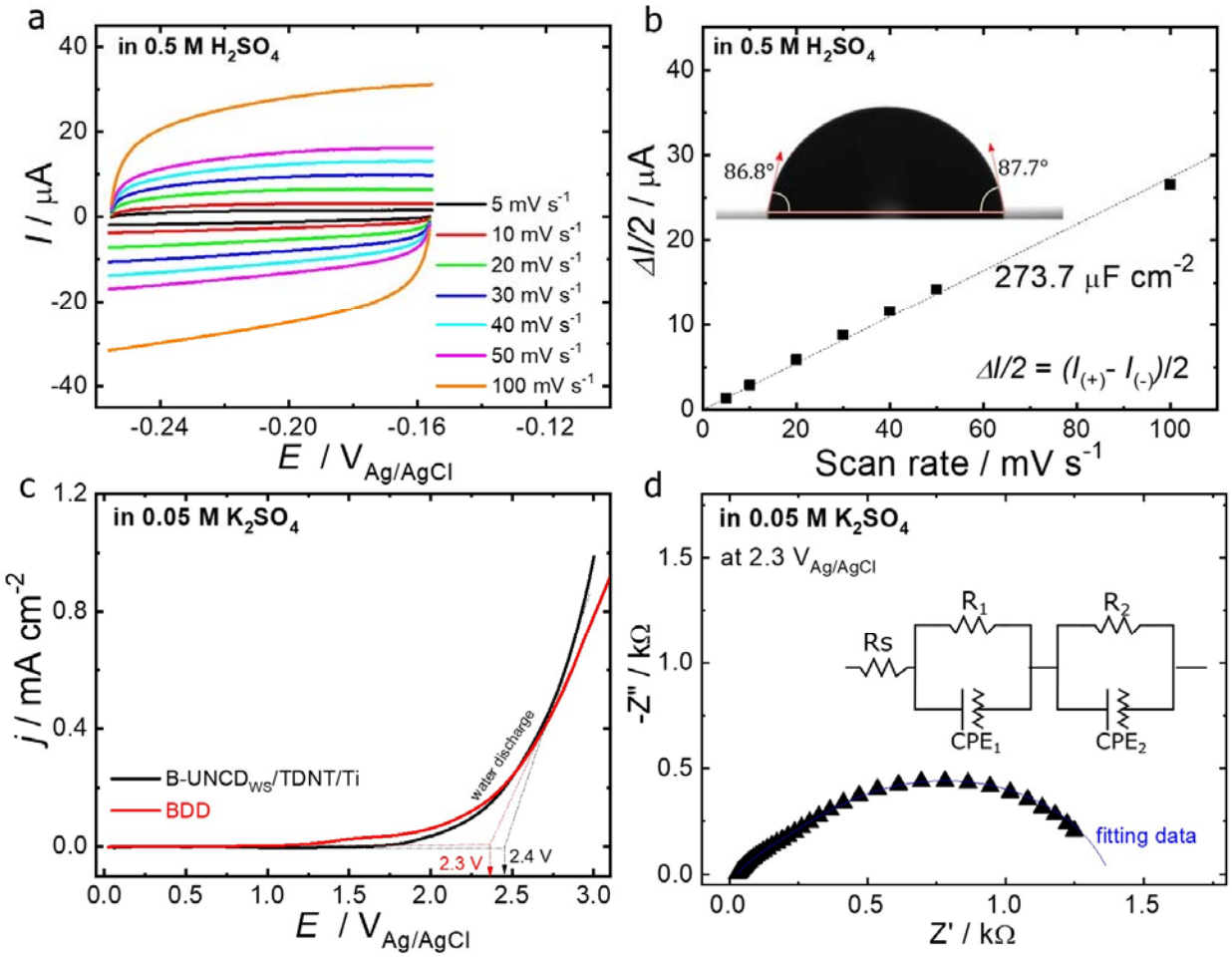

Fig 2. Electrochemical characterization of the B-UNCD$_{WS}$/TDNT/Ti electrode. (a) Cyclic voltammograms obtained from the application of N_2-saturated 0.5 M H_2SO_4 as supporting electrolyte at different scan rates. (b) $\Delta I/2$ *vs.* scan rate plot; inset: water contact angle measurement. (c) LSV curves for B-UNCD$_{WS}$/TDNT/Ti and commercial BDD electrodes obtained in N_2-saturated 0.05 M K_2SO_4 (employed as supporting electrolyte) and scan rate of 20 mV s^{-1}. The scan started at 0 V *vs.* Ag/AgCl. (d) Complex-impedance plane representation; inset: simulated electric equivalent circuit (EEQC).

Fig. 2d shows the complex-impedance plot obtained for the B-UNCD$_{WS}$/TDNT/Ti electrode in N_2–saturated 50 mM K_2SO_4 close to the water discharge onset potential. The EIS response revealed the capacitive–resistive character of the ultrananо-diamond electrode, which is characterized by two structural layers linked to the presence of TDNT/Ti. The simulated electric equivalent circuit (EEQC) can be represented by a resistance related to the electrolyte and two RQ components, where both are connected in series (Ennaceri et al., 2020) (R(RQ)(RQ) circuit, c.f. inset of Fig. 2d). The first RQ component is associated with large porous

225 spherical ultranano-diamond structures; these structures consist of a charge transfer resistance and a constant
226 phase element (CPE) which is linked to the double layer capacitance (Almeida et al., 2008). The second RQ
227 component, which exhibits a more resistive character, is linked to porous TDNT which is finely coated by
228 ultranano-diamond film probably with some exposed TDNT dots (Ennaceri et al., 2020). The results obtained
229 from the physical and electrochemical characterization analyses show that the B-$UNCD_{WS}$/TDNT/Ti electrode
230 has outstanding physical-chemical properties, and this makes it highly suitable for application in
231 electrocatalytic water technologies as will be discussed in the next section.
232
233 *3.2. Electrochemical treatment of CBR using the B-$UNCD_{WS}$/TDNT/Ti anode.*
234 In electrochemical advanced oxidative processes (EAOPs), current density (*j*) is an essentially important
235 electrokinetic parameter; this parameter controls the quantity of electrons circulating in the system, and
236 consequently, the amount of $^{\bullet}OH$ that can be generated. Bearing that in mind, the efficiency of the *B-*
237 *$UNCD_{WS}$/TDNT/Ti* anode was assessed based on the application of different current densities for the treatment
238 of 10 mg L^{-1} of carbaryl (CBR) in 50 mM K_2SO_4 (used as supporting electrolyte) at pH = 7.0. Looking at the
239 results shown in Fig. 3a, one will observe that the application of the *B-$UNCD_{WS}$/TDNT/Ti* anode effectively
240 resulted in CBR degradation irrespective of the current density applied. Interestingly though, after 30 min of
241 treatment, there were changes in the degradation pattern. The following degradation rates (in decreasing order)
242 were obtained under the application of different current densities: 75 mA cm^{-2} (99.9 %) > 100 mA cm^{-2} (97.5
243 %) > 50 mA cm^{-2} (69.9 %) > 25 mA cm^{-2} (27.8 %). An approximately 9-fold increase was observed in CBR
244 degradation from the current density of 25 to 75 mA cm^{-2} over time; this was certainly due to the increase in
245 the amount of $^{\bullet}OH$ generated in the electrolysis (Eq. (1)). However, the two highest applied current densities
246 (75 and 100 mA cm^{-2}) exhibited a quite similar behavior in terms of CBR removal; this behavior can be
247 attributed to the presence of parasitic/non-oxidative reactions. Indeed, the occurrence of parasitic reactions is
248 favored by the increase in current density due to the competition between $^{\bullet}OH$ with O_2 evolution (Eq. (4)).
249 Another point worth mentioning is that due to its non-selective character, $^{\bullet}OH$ can react with each other
250 (dimerization reaction), producing hydrogen peroxide (H_2O_2), which is a weaker oxidant compared to $^{\bullet}OH$ –
251 see reaction 5 below (Brillas et al., 2010; Srivastava et al., 2021). Both reactions 4 and 5 decrease the oxidative
252 power of the system once they consume $^{\bullet}OH$.

253 $2^{\bullet}OH \rightarrow O_2 + 2H^+ + 2e^-$ (4)

254 $2^{\bullet}OH \rightarrow H_2O_2$ (5)

255 From the viewpoint of the applied charge, the pattern of CBR degradation shown in Fig. 3b is quite similar
256 to that observed in Fig. 3a. At 0.33 Ah L^{-1}, the final CBR concentrations obtained from the application of
257 current densities of 25, 50, 100 and 75 mA cm^{-2} were 4.87, 3.01, 2.81, 1.16 mg L^{-1}, respectively. In fact, the
258 optimal *j* value that promoted a complete removal of CBR was 75 mA cm^{-2}, with charge consumption of 0.50
259 Ah L^{-1}; for comparison purposes, the application of the current density of 100 mA cm^{-2} requires charge
260 consumption of 0.84 Ah L^{-1} to obtain a complete removal of CBR. Taking a closer look at the relationship
261 between the pseudo-first-order kinetics constant (k_1) and EE/O (Fig. 3c), one will observe that when k_1
262 increases, EE/O decreases – see the following results obtained at different current densities: 25 mA cm^{-2}
263 ($2.1x10^{-4}$ s^{-1}, $R^2 = 0.994$; 6.90 kWh m^{-3} $order^{-1}$), 50 mA cm^{-2} ($7.4x10^{-4}$ s^{-1}, $R^2 = 0.991$; 5.87 kWh m^{-3} $order^{-1}$),
264 100 mA cm^{-2} ($1.8x10^{-3}$ s^{-1}, $R^2 = 0.983$; 6.44 kWh m^{-3} $order^{-1}$) and 75 mA cm^{-2} ($1.9x10^{-3}$ s^{-1}, $R^2 = 0.987$; 4.01
265 kWh m^{-3} $order^{-1}$). These results clearly show that high *j* values are required for the effective degradation of
266 CBR; in essence, this finding shows that there is a mass transfer mechanism controlled by diffusion in which
267 the porosity plays a fundamental role by increasing the anode effective surface and favoring the pollutants-
268 oxidant contact. The supply of energy above $j = 75$ mA cm^{-2} does not translate into better performance and
269 greater cost-effectiveness of the process, as observed in Figs. 3a-c. In fact, the application of current densities
270 above 75 mA cm^{-2} may fuel the occurrence of non-oxidizing reactions as previously discussed; in contrast, the
271 application of current densities below 75 mA cm^{-2} may cause resistance in the system probably due to the low
272 level of boron on the anode surface. Thus, the current density of 75 mA cm^{-2} was selected for the conduct of
273 further experiments.

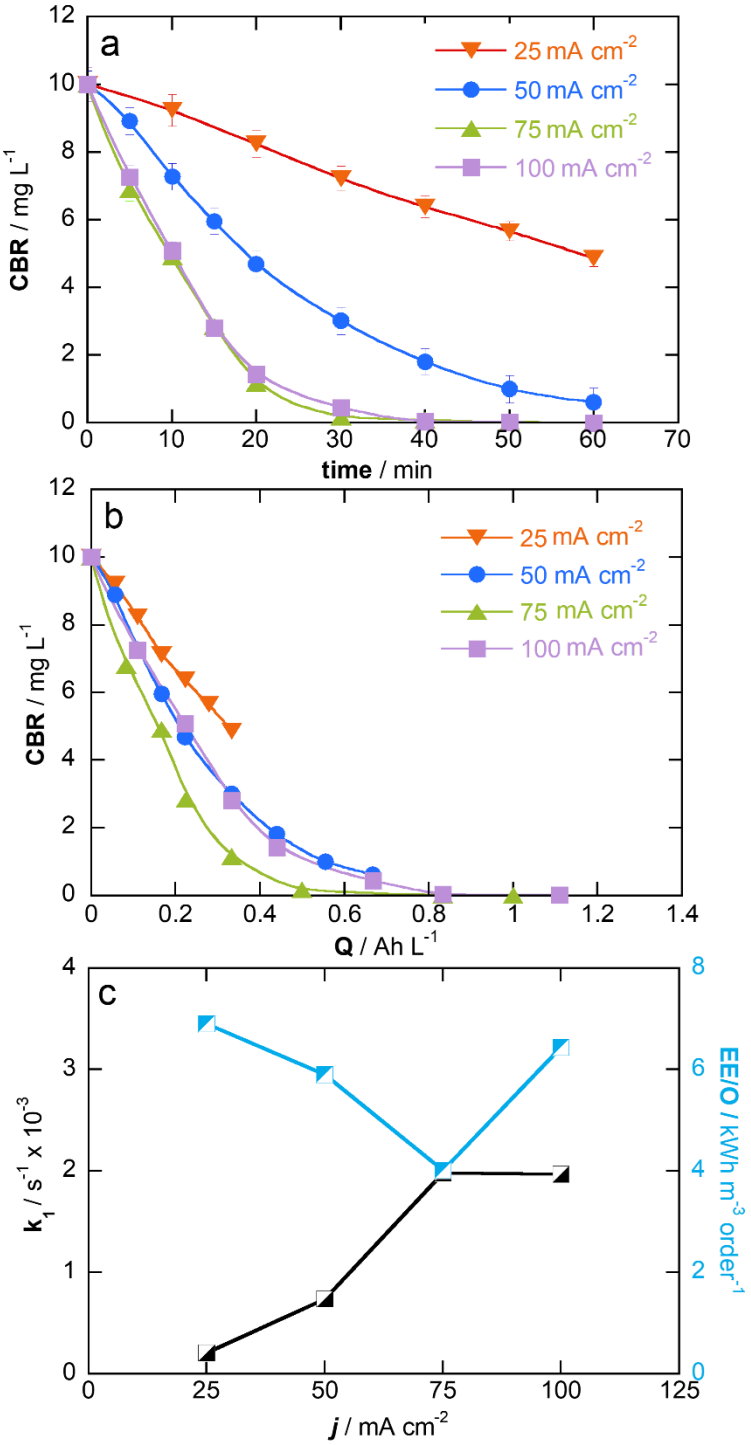

Fig 3. Effect of current density on the degradation of CBR concentration relative to (a) electrolysis time and (b) applied charge. (c) Pseudo-first order kinetic decay of CBR and electrical energy per order versus current density. Operating conditions:10 mg L^{-1} of CBR; 50 mM of K_2SO_4 (used as supporting electrolyte) at pH = 7.0.

The AO process allows the in-situ generation of radical species. To gain a meaningful understanding regarding the contribution of these radical species in the degradation of CBR, TBH was used to scavenge $^{\bullet}OH$, while MeOH was used to scavenge $^{\bullet}OH$ and $SO_4^{\bullet-}$. Different pollutant:scavenger ratios (1:50, 1:100, 1:200, 1:400) were used to find the optimal testing concentration. The k_1 values obtained for CBR removal were found to be influenced by the presence of scavengers up to the ratio 1:200; the values then remained constant at higher concentrations – after 1:200 (data not shown). So, when the ratio of 1:200 was employed, the application of the TBH and MeOH scavengers led to a reduction in the k_1 value from 1.9×10^{-3} s^{-1} to 2.9×10^{-4} s^{-1} and 1.8×10^{-4} s^{-1} (Fig. 4a), respectively. A careful analysis of these results showed that $^{\bullet}OH$ - the main oxidant, represented 84.7% of the results (= 100 × ($k_{1,control}$ - $k_{1,TBH}$)/$k_{1,control}$), while $SO_4^{\bullet-}$ represented only 5.8% (($k_{1,TBH}$ - $k_{1,MeOH}$)/$k_{1,control}$), and the rest accounted for 9.5%. It should be noted that $SO_4^{\bullet-}$ can be electrogenerated through direct oxidation via one-electron of sulfate - see Eq. (6). The remaining 9.5% can be attributed to non-radical oxidation which is associated with the direct oxidation of the pollutant and persulfate activation - both phenomena occurring on the anode surface (Song et al., 2018).

$$SO_4^{2-} \rightarrow SO_4^{\bullet-} + e^- \quad (6)$$

The stability of the *B-UNCD$_{WS}$/TDNT/Ti* electrode for longer operation periods was evaluated using five consecutive fed-batch tests of 60 min duration. During all the tests, the operating conditions were kept unchanged. As can be seen in Fig. 4b, the carbaryl removal rate was practically the same (around 100%) for the first five tests; this result points to the efficient performance and long-term stability of the *B-UNCD$_{WS}$/TDNT/Ti* electrode applied for the degradation of recalcitrant compounds in water.

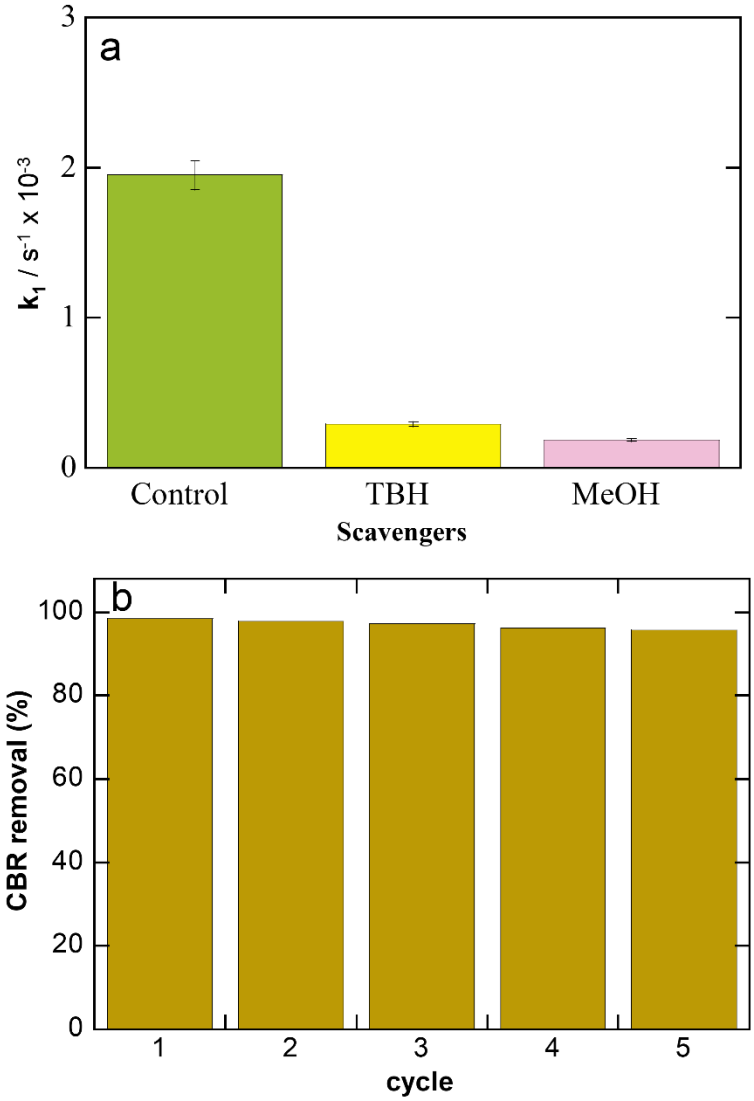

299 **Fig 4.** (a) Effect of the application of different scavengers on the pseudo-first order kinetic decay of CBR.
300 (b) Effect of the B-UNCD$_{WS}$/TDNT/Ti electrode on CRB removal over 5 cycles of electrolysis. Operating
301 conditions: 10 mg L^{-1} of CBR; 50 mM of K_2SO_4 at pH = 7.0 (employed as supporting electrolyte).
302
303 Although complete CBR degradation was obtained, the environmental problem has still not yet to be
304 addressed. In certain treatment processes, the final by-products obtained after the treatment are found to be
305 more persistent than the original pollutant. In view of that, a thorough analysis was performed to study the
306 mineralization process (≈ 95% - data not shown) and identify/quantify the final by-products generated after
307 the pollutant treatment process. Fig 5a shows the time-course of the evolution of the concentration of short
308 linear carboxylic acids derived from the opening of the naphthalene group present in the CBR. The results
309 obtained from the mineralization analysis pointed to the presence of a mixture of oxalic, fumaric, formic, and

310 acetic acids, with maximum concentrations of 0.496 mg L^{-1} (120 min), 0.061 mg L^{-1} (60 min), 0.835 mg L^{-1}
311 (120 min) and 0.295 mg L^{-1} (180 min), respectively, which were partially converted to CO_2, with the exception
312 of the fumaric acid which was completely mineralized. In addition, an analysis was also performed in order to
313 study the evolution of nitrogenous ions – see the results obtained in Fig. 5b. Looking at the results shown in
314 Fig 5b, one will observe that the initial amount of nitrogen in the CBR (0.649 mg L^{-1}) was mostly converted
315 to ammonia (0.62 mg L^{-1} - 74.30%), followed by nitrate (0.23 mg L^{-1} - 8.32%) and nitrite (0.026 mg L^{-1} -
316 1.23%). The remaining 16.15% of the total mass was probably related to volatile N-products, as reported in
317 previous studies (Çelebi et al., 2015; Oriol et al., 2021). Depending on their concentration levels, the exposure
318 to nitrate, nitrite, and ammonia ions may pose serious risks to human health. However, it is worth mentioning
319 that the remaining concentrations of nitrate and nitrite after the electrochemical treatment were found to be
320 below the maximum contamination level (MCL) stipulated for drinking water according to the US
321 Environmental Protection Agency (EPA): 10.0 and 1.0 mg N L^{-1}, respectively. According to the same agency,
322 there is no legally established MCL for ammonia.

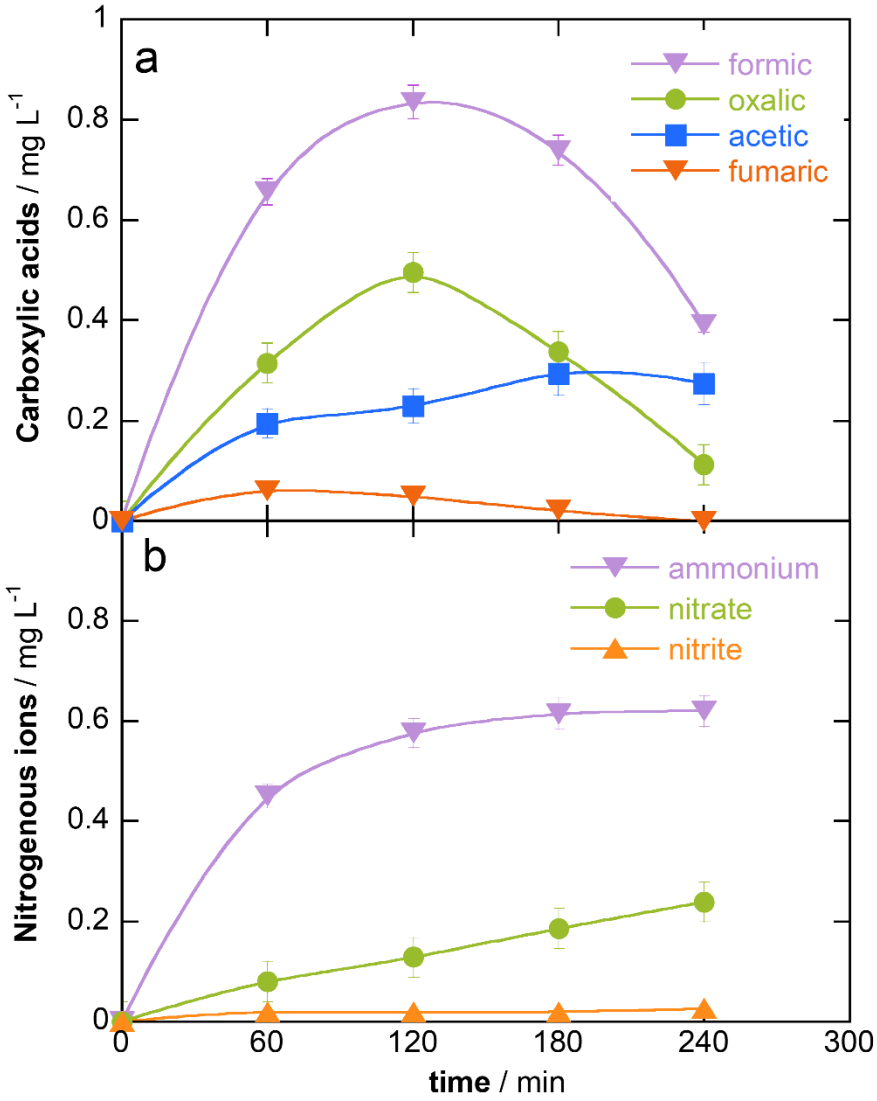

Fig 5. Time course of the evolution of (a) short linear carboxylic acids and (b) nitrogenous species during the treatment of 10 mg L-1 of CBR in 50 mM K2SO4 , with pH = 7.0 (employed as supporting electrolyte), and j = 75 mA cm^{-2}.

3.3. Electrochemical treatment of CBR in real medium

Clearly, the experiments conducted using ultrapure water helped us understand the degree of efficiency of the treatment process applied in this study and its mechanism of operation for the removal of CBR in synthetic medium. However, conducting experiments in synthetic aqueous medium alone is not sufficient for us to have a more realistic understanding of the treatment process and the impact of the presence of other compounds (i.e., inorganic ions, natural organic matter) on the pollutant degradation. Thus, based on the satisfactory results obtained from the experiments conducted using synthetic medium, we evaluated the efficiency of the *B*-

335 *UNCDWS/TDNT/Ti* anode when applied for the treatment of real effluents. The analysis was conducted using
336 the optimal current density of 75 mA cm^{-2} in real drinking water spiked with different concentrations of CBR
337 (5.0 – 20 mg L^{-1}). As can be observed in Fig. 6, irrespective of the initial concentration of CBR, there was a
338 sharp decrease in the pollutant concentration in the first 15 min of reaction; thereafter, the decrease in the
339 pollutant concentration took a more gradual pattern. The initial concentration of CBR is a parameter of interest
340 since it provides one with fundamental information regarding the range of pollutant concentration that can be
341 efficiently treated in reasonable periods of time. For instance, in 30 min of treatment, the pollutant removal
342 rates obtained were 99.8 %, 93.5 % and 89.4% for the initial concentrations of 5.0, 10, and 20 mg L^{-1},
343 respectively.

344 The analysis of real water samples shows the presence of other compounds besides the pollutant and the
345 electrolyte, and this can positively or negatively affect the removal of the contaminant. A comparison of the
346 results obtained from the experiments conducted using real effluent with the results obtained from the
347 experiments conducted using synthetic medium under the same operating conditions showed that the span of
348 time required to obtain a complete removal of the pollutant was 1.2 times higher in the real effluent than in the
349 synthetic medium (with a reduction of k_1 from $1.9x10^{-3}$ s-1 to $1.6x10^{-3}$ for the experiment in real effluent and
350 in synthetic medium, respectively). The presence of natural organic matter in the real medium (Table 1)
351 competes for the electrogenerated oxidants, undermining the efficiency of the process. On the other hand, the
352 presence of chloride in real medium allows the electrogeneration of active chlorine species ($Cl_{2(aq)}$ – Eq. (7);
353 HClO – Eq. (8); OCl^- – Eq. (9)), which may enhance the performance of the system. Generally, these species
354 are generated at the following pH levels: pH ≤ 3 (Cl_2(aq)), pH range 3-8 (HClO), and pH > 8 (ClO^-). Thus, the
355 oxidation of organic matter mediated by active chlorine species is found to be stronger in acidic than in alkaline
356 media due to the higher standard potential of Cl_2(aq) (E°= 1.36 *vs* SHE) and HClO (E°= 1.49 *vs* SHE) compared
357 to that of ClO^- (E°= 0.89 *vs* SHE) (Burgos-Castillo et al., 2018; Garcia-Segura et al., 2018b). However, it
358 seems that the presence of chlorine species in the medium did not have such a significant impact on CBR
359 removal; this was probably because of the low initial concentration of chloride, which was not enough to
360 induce the electrogeneration of high amount of active chlorine species. It is interesting to note that at the end
361 of the experiment, no chloro oxyanions, such as chlorate and perchlorate, were detected in the solution; this is
362 evidently reassuring because these species are carcinogenic.

363 $2Cl^- \rightarrow Cl_{2(aq)} + 2e^-$ (7)

364 $Cl_{2(aq)} + H_2O \rightarrow HClO + Cl^- + H^+$ (8)

365 $HClO \leftrightarrows ClO^- + H^+ \quad pK_a = 7.55$ (9)

366

367 With regard to the mineralization tests performed using the real effluent (Fig. 6b), the results obtained showed
368 that none of the experiments yielded 100% removal rates. In fact, at the end of the treatment, TOC removal
369 rates of 52.3, 58.7 and 65.2% were obtained for the tests conducted using 5, 10 and 20 mg L^{-1} of CBR,
370 respectively. Increasing the concentration of CBR may lead to the generation and accumulation of a huge
371 number of intermediates and by-products, and these additional compounds compete with the pollutant
372 molecules to react with the same amount of $^{\bullet}OH$ radicals, thus decreasing the removal efficiency of the process.
373 It is worth pointing out that the pattern of TOC removal was found to be entirely different from that observed
374 in CBR degradation. In the mineralization experiments, the removal efficiency was found to be higher for the
375 test with higher initial CBR concentration. The mineralization phenomenon is boosted in the presence of higher
376 organic load, diminishing the extent/magnitude of parasitic reactions. Based on the results obtained in this
377 study, it is clear that the *B-UNCD$_{WS}$/TDNT/Ti* electrode has proven to be highly efficient when applied for the
378 removal of different concentrations of CBR. Regarding CBR mineralization, the application of the proposed
379 electrode was found to require longer treatment times to obtain satisfactory results; still, the TOC removal
380 rates of 52.3– 65.5 % obtained in 60 min of treatment are found to be reasonable considering that this is the
381 first time the proposed electrode has been employed for CBR degradation. The encouraging results obtained
382 in this study (based on the application of the proposed electrode for CBR removal) can be most likely attained
383 when the proposed technique is applied for the treatment of other recalcitrant water pollutants.

384

385

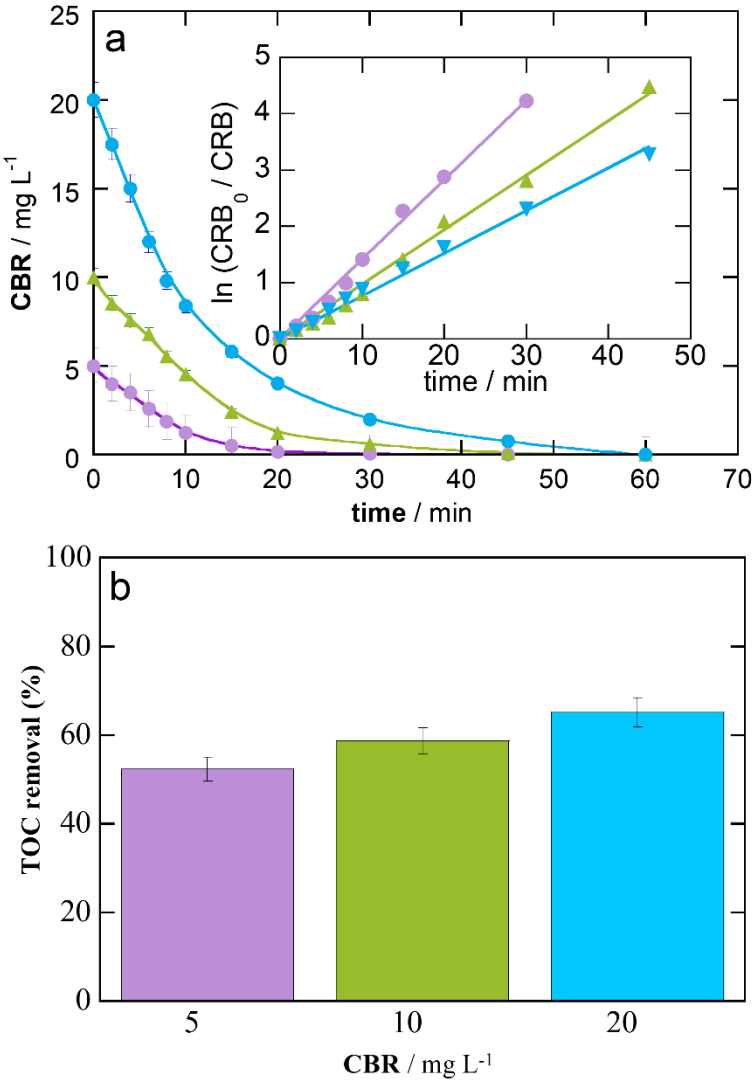

Fig 6. (a) Carbaryl degradation over time and (b) mineralization after 60 min treatment of real water with different CBR concentrations at current density of 75 mA cm^{-2}.

4. Conclusions

The present work reported the synthesis of B-UNCD$_{WS}$/TDNT/Ti electrodes with extremely thin diamond films using an innovative methodology without seeding substrate pre-treatment and their successful application for the treatment of water containing recalcitrant compounds. The material proposed in this study was found to possess suitable electrochemical properties, including highly porous ultrananо-structures, improved specific capacitance (274 μF cm^{-2}) and high onset potential for water discharge (ca. 2.4 V *vs.* Ag/AgCl); these properties favored the generation of reactive oxygen species during the electrolysis process. Owing to the combination of the aforementioned properties, the application of the proposed electrode at the current density of 75 mA cm^{-2} contributed effectively toward the complete removal of CBR in synthetic medium in 30 min (Q=0.5 Ah L^{-1}) with electric energy consumption per order of 4.01 kWh m^{-3} order^{-1}. The use of scavengers in the treatment process helped confirm that $^{\bullet}$OH was the main oxidant species (with effective contribution of ≈ 84.7%) that took part in the degradation of the pollutant. The results obtained from the analysis of the final by-products of the electrolysis pointed to the presence of carboxylic acids, including acetic, formic, fumaric and oxalic acids, but zero or minimal concentrations of these acids were detected at the end of the electrochemical treatment. The concentrations of nitrogenated species monitored over the treatment period were found to be within the maximum contamination level for drinking water; this evidently helps reduce the health risks posed by the presence of these substances in water. The results obtained from the application of the proposed electrode for the removal of CBR in real effluents were found to be satisfactory; complete degradation was obtained within 20-60 min treatment of effluents containing 5 – 20 mg L^{-1} of CBR while TOC removal rates of 52.3– 65.5 % were obtained after 60 min of treatment. This work highlights the advantages of improving the synthesis of BDD electrode and its contribution toward enhancing the effectiveness and competitiveness of electrochemical advanced oxidation processes when applied for the degradation of recalcitrant pollutants.

Acknowledgments

The authors acknowledge the financial support provided by the following Brazilian research funding agencies: Brazilian National Council for Scientific and Technological Development - CNPq (grant #465571/2014-0and #303943/2021-1), São Paulo Research Foundation - FAPESP (grants #2014/50945-4, #2017/23464-3, #2017/10118-0, #2019/04421-7, #2019/20634-0, #2019/00592-1 and #2021/07615-7) and the Coordenação de Aperfeiçoamento de Pessoal de Nível Superior (CAPES – Finance Code 001) in support of this work. Haruna L. Barazorda-Ccahuana is grateful for the financial assistance received in support of the internal project UCSM 7309-CU-2020. Dr. Ana S. Fajardo is likewise grateful for the funding granted by the European Union Horizon 2020 research and innovation program under the Marie Sklodowska-Curie grant agreement No 843870.

References

Almeida, E.C., Baldan, M.R., Rosolen, J.M., Ferreira, N.G., 2008. Impedance characteristics of the diamond/carbon fiber electrodes for electrical double-layer capacitor. Diam. Relat. Mater. 17, 1529–1533. https://doi.org/10.1016/j.diamond.2008.03.006

Baddouh, A., Bessegato, G.G., Rguiti, M.M., El Ibrahimi, B., Bazzi, L., Hilali, M., Zanoni, M.V.B., 2018. Electrochemical decolorization of Rhodamine B dye: Influence of anode material, chloride concentration and current density. J. Environ. Chem. Eng. 6, 2041–2047. https://doi.org/10.1016/j.jece.2018.03.007

Baluchová, S., Taylor, A., Mortet, V., Sedláková, S., Klimša, L., Kopeček, J., Hák, O., Schwarzová-Pecková, K., 2019. Porous boron doped diamond for dopamine sensing: Effect of boron doping level on morphology and electrochemical performance. Electrochim. Acta 327, 135025. https://doi.org/10.1016/j.electacta.2019.135025

Brillas, E., 2021. Recent development of electrochemical advanced oxidation of herbicides. A review on its application to wastewater treatment and soil remediation. J. Clean. Prod. 290, 125841. https://doi.org/10.1016/j.jclepro.2021.125841

Brillas, E., Garcia-Segura, S., Skoumal, M., Arias, C., 2010. Electrochemical incineration of diclofenac in neutral aqueous medium by anodic oxidation using Pt and boron-doped diamond anodes. Chemosphere 79, 605–612. https://doi.org/10.1016/j.chemosphere.2010.03.004

Burgos-Castillo, R.C., Sirés, I., Sillanpää, M., Brillas, E., 2018. Application of electrochemical advanced oxidation to bisphenol A degradation in water. Effect of sulfate and chloride ions. Chemosphere 194, 812–820. https://doi.org/10.1016/j.chemosphere.2017.12.014

Çelebi, M.S., Oturan, N., Zazou, H., Hamdani, M., Oturan, M.A., 2015. Electrochemical oxidation of carbaryl on platinum and boron-doped diamond anodes using electro-Fenton technology. Sep. Purif. Technol. 156, 996–1002. https://doi.org/10.1016/j.seppur.2015.07.025

Crisci, A., Mermoux, M., Saubat-Marcus, B., 2008. Deep ultra-violet Raman imaging of CVD boron-doped and non-doped diamond films. Diam. Relat. Mater. 17, 1207–1211. https://doi.org/10.1016/j.diamond.2008.01.025

453 do Vale□Júnior, E., dos Santos, A.J., da Silva, D.R., Fajardo, A.S., Martínez□Huitle, C.A., 2019.
454 Electrochemical technologies for detecting and degrading benzoquinone using diamond films.
455 ChemElectroChem 6, 4383–4390. https://doi.org/10.1002/celc.201900541
456 dos Santos, A.J., Fajardo, A.S., Kronka, M.S., Garcia-Segura, S., Lanza, M.R.V., 2021a. Effect of
457 electrochemically-driven technologies on the treatment of endocrine disruptors in synthetic and real
458 urban wastewater. Electrochim. Acta 376, 138034. https://doi.org/10.1016/j.electacta.2021.138034
459 dos Santos, A.J., Fortunato, G. V., Kronka, M.S., Vernasqui, L.G., Ferreira, N.G., Lanza, M.R.V., 2022.
460 Electrochemical oxidation of ciprofloxacin in different aqueous matrices using synthesized boron-
461 doped micro and nano-diamond anodes. Environ. Res. 204, 112027.
462 https://doi.org/10.1016/j.envres.2021.112027
463 dos Santos, A.J., Garcia-Segura, S., Dosta, S., Cano, I.G., Martínez-Huitle, C.A., Brillas, E., 2019. A ceramic
464 electrode of ZrO_2-Y_2O_3 for the generation of oxidant species in anodic oxidation. Assessment of the
465 treatment of Acid Blue 29 dye in sulfate and chloride media. Sep. Purif. Technol. 228, 115747.
466 https://doi.org/10.1016/j.seppur.2019.115747
467 dos Santos, A.J., Kronka, M.S., Fortunato, G. V., Lanza, M.R.V., 2021b. Recent advances in electrochemical
468 water technologies for the treatment of antibiotics: A short review. Curr. Opin. Electrochem. 26,
469 100674. https://doi.org/10.1016/j.coelec.2020.100674
470 Ennaceri, H., Fischer, K., Hanus, K., Chemseddine, A., Prager, A., Griebel, J., Kühnert, M., Schulze, A.,
471 Abel, B., 2020. Effect of morphology on the photoelectrochemical activity of TIO_2 self-organized
472 nanotube arrays. Catalysts 10, 279. https://doi.org/10.3390/catal10030279
473 Frackowiak, E., Béguin, F., 2001. Carbon materials for the electrochemical storage of energy in capacitors.
474 Carbon N. Y. 39, 937–950. https://doi.org/10.1016/S0008-6223(00)00183-4
475 Garcia-Segura, S., Lanzarini-Lopes, M., Hristovski, K., Westerhoff, P., 2018a. Electrocatalytic reduction of
476 nitrate: Fundamentals to full-scale water treatment applications. Appl. Catal. B: Environ. 236, 546–
477 568. https://doi.org/10.1016/j.apcatb.2018.05.041
478 Garcia-Segura, S., Ocon, J.D., Chong, M.N., 2018b. Electrochemical oxidation remediation of real
479 wastewater effluents — A review. Process Saf. Environ. Prot. 113, 48–67.
480 https://doi.org/10.1016/j.psep.2017.09.014

Kapałka, A., Fóti, G., Comninellis, C., 2009. The importance of electrode material in environmental electrochemistry. Electrochim. Acta 54, 2018–2023. https://doi.org/10.1016/j.electacta.2008.06.045

Kapałka, A., Fóti, G., Comninellis, C., 2007. Kinetic modelling of the electrochemical mineralization of organic pollutants for wastewater treatment. J. Appl. Electrochem. 38, 7–16. https://doi.org/10.1007/s10800-007-9365-6

Karim, A. V., Nidheesh, P.V., Oturan, M.A., 2021. Boron-doped diamond electrodes for the mineralization of organic pollutants in the real wastewater. Curr. Opin. Electrochem. 30, 100855. https://doi.org/10.1016/j.coelec.2021.100855

Koshlukova, S.E., Reed, N.R., 2014. Carbaryl, in: Encyclopedia of toxicology. Elsevier, pp. 668–672. https://doi.org/10.1016/B978-0-12-386454-3.00107-X

Lanzarini-Lopes, M., Garcia-Segura, S., Hristovski, K., Westerhoff, P., 2017. Electrical energy per order and current efficiency for electrochemical oxidation of p-chlorobenzoic acid with boron-doped diamond anode. Chemosphere 188, 304–311. https://doi.org/10.1016/j.chemosphere.2017.08.145

Luong, J.H.T., Male, K.B., Glennon, J.D., 2009. Boron-doped diamond electrode: synthesis, characterization, functionalization and analytical applications. Analyst 134, 1965. https://doi.org/10.1039/b910206j

Macpherson, J. V., 2015. A practical guide to using boron doped diamond in electrochemical research. Phys. Chem. Chem. Phys. 17, 2935–2949. https://doi.org/10.1039/C4CP04022H

Martínez-Huitle, C.A., Panizza, M., 2018. Electrochemical oxidation of organic pollutants for wastewater treatment. Curr. Opin. Electrochem. 11, 62–71. https://doi.org/10.1016/j.coelec.2018.07.010

May, P.W., Mankelevich, Y.A., 2008. From ultrananocrystalline diamond to single crystal diamond growth in hot filament and microwave plasma-enhanced CVD reactors: A unified model for growth rates and grain sizes. J. Phys. Chem. C 112, 12432–12441. https://doi.org/10.1021/jp803735a

McCrory, C.C.L., Jung, S., Peters, J.C., Jaramillo, T.F., 2013. Benchmarking heterogeneous electrocatalysts for the oxygen evolution reaction. J. Am. Chem. Soc. 135, 16977–16987. https://doi.org/10.1021/ja407115p

Mei, R., Wei, Q., Zhu, C., Ye, W., Zhou, B., Ma, L., Yu, Z., Zhou, K., 2019. 3D macroporous boron-doped diamond electrode with interconnected liquid flow channels: A high-efficiency electrochemical

degradation of RB-19 dye wastewater under low current. Appl. Catal. B Environ. 245, 420–427. https://doi.org/10.1016/j.apcatb.2018.12.074

Mermoux, M., Marcus, B., Swain, G.M., Butler, J.E., 2002. A confocal raman imaging study of an optically transparent boron-doped diamond electrode. J. Phys. Chem. B 106, 10816–10827. https://doi.org/10.1021/jp0202946

Moreira, F.C., Boaventura, R.A.R., Brillas, E., Vilar, V.J.P., 2017. Electrochemical advanced oxidation processes: A review on their application to synthetic and real wastewaters. Appl. Catal. B Environ. 202, 217–261. https://doi.org/10.1016/j.apcatb.2016.08.037

Mostafa, E., Baltruschat, H., Garcia-Segura, S., 2021. Unraveling the role of electrolytes during electrochemical oxidation by differential electrochemical mass spectrometry. Electrochim. Acta 387, 138521. https://doi.org/10.1016/j.electacta.2021.138521

Nair, S.R., Menacherry, S.P.M., Renjith, S., Manojkumar, T.K., Aravind, U.K., Aravindakumar, C.T., 2022. Oxidation reactions of carbaryl in aqueous solutions. Chem. Phys. 554, 111427. https://doi.org/10.1016/j.chemphys.2021.111427

Oriol, R., Brillas, E., Cabot, P.L., Cortina, J.L., Sirés, I., 2021. Paired electrochemical removal of nitrate and terbuthylazine pesticide from groundwater using mesh electrodes. Electrochim. Acta 383, 138354. https://doi.org/10.1016/j.electacta.2021.138354

Ownby, P.D., Yang, X., Liu, J., 1992. Calculated x-ray diffraction data for diamond polytypes. J. Am. Ceram. Soc. 75, 1876–1883. https://doi.org/10.1111/j.1151-2916.1992.tb07211.x

Panizza, M., Cerisola, G., 2009. Direct And Mediated Anodic Oxidation of Organic Pollutants. Chem. Rev. 109, 6541–6569. https://doi.org/10.1021/cr9001319

Sirés, I., Brillas, E., 2012. Remediation of water pollution caused by pharmaceutical residues based on electrochemical separation and degradation technologies: A review. Environ. Int. 40, 212–229. https://doi.org/10.1016/j.envint.2011.07.012

Sirés, I., Brillas, E., Oturan, M.A., Rodrigo, M.A., Panizza, M., 2014. Electrochemical advanced oxidation processes: today and tomorrow. A review. Environ. Sci. Pollut. Res. 21, 8336–8367. https://doi.org/10.1007/s11356-014-2783-1

Siuzdak, K., Bogdanowicz, R., Sawczak, M., Sobaszek, M., 2015. Enhanced capacitance of composite TiO_2 nanotube/boron-doped diamond electrodes studied by impedance spectroscopy. Nanoscale 7, 551–558. https://doi.org/10.1039/C4NR04417G

Song, H., Yan, L., Jiang, J., Ma, J., Zhang, Z., Zhang, J., Liu, P., Yang, T., 2018. Electrochemical activation of persulfates at BDD anode: Radical or nonradical oxidation? Water Res. 128, 393–401. https://doi.org/10.1016/j.watres.2017.10.018

Srivastava, V., Suresh Kumar, M., Nidheesh, P.V., Martínez-Huitle, C.A., 2021. Electro catalytic generation of reactive species at diamond electrodes and applications in microbial inactivation. Curr. Opin. Electrochem. 30, 100849. https://doi.org/10.1016/j.coelec.2021.100849

Szunerits, S., Coffinier, Y., Boukherroub, R., 2015. Diamond Nanowires: a novel platform for electrochemistry and matrix-free mass spectrometry. Sensors 15, 12573–12593. https://doi.org/10.3390/s150612573

Vernasqui, L.G., Kawata, B.A., Sardinha, A.F., Rodrigo, M.A., Ferreira, N.G., 2022. Achievement and electrochemical responsiveness of advanced boron-doped ultrananocrystalline diamond on highly ordered titanium dioxide nanotubes. Diam. Relat. Mater. 121, 108793. https://doi.org/10.1016/j.diamond.2021.108793

Watanabe, T., Shimizu, T.K., Tateyama, Y., Kim, Y., Kawai, M., Einaga, Y., 2010. Giant electric double-layer capacitance of heavily boron-doped diamond electrode. Diam. Relat. Mater. 19, 772–777. https://doi.org/10.1016/j.diamond.2010.02.022

Wei, M., Terashima, C., Lv, M., Fujishima, A., Gu, Z.-Z., 2009. Boron-doped diamond nanograss array for electrochemical sensors. Chem. Commun. 3624. https://doi.org/10.1039/b903284c

Wu, P., Xie, L., Mo, W., Wang, B., Ge, H., Sun, X., Tian, Y., Zhao, R., Zhu, F., Zhang, Y., Wang, Y., 2019. The biodegradation of carbaryl in soil with Rhodopseudomonas capsulata in wastewater treatment effluent. J. Environ. Manage. 249, 109226. https://doi.org/10.1016/j.jenvman.2019.06.127

Yang, N., Foord, J.S., Jiang, X., 2016. Diamond electrochemistry at the nanoscale: A review. Carbon N. Y. 99, 90–110. https://doi.org/10.1016/j.carbon.2015.11.061